Author Manuscript

Author Manuscript

Author Manuscript

Author Manuscript

HHS Public Access

Author manuscript

Nat Chem. Author manuscript; available in PMC 2022 July 01.

Published in final edited form as:

Nat Chem. 2022 January ; 14(1): 100–109. doi:10.1038/s41557-021-00803-1.

Native Mass Spectrometry based Metabolomics Identifies Metal-binding Compounds

Allegra T. Aron[1,2,*], **Daniel Petras**[1,2,3,12,*], **Robin Schmid**[1,4], **Julia M. Gauglitz**[1,2,11], **Isabell Büttel**[5], **Luis Antelo**[6], **Hui Zhi**[7], **Sean-Paul Nuccio**[7], **Christina C. Saak**[10], **Kien P. Malarney**[10], **Eckhard Thines**[5,6], **Rachel J. Dutton**[9,10], **Lihini I. Aluwihare**[3], **Manuela Raffatellu**[7,8,9], **Pieter C. Dorrestein**[1,3,9,#]

[1]Skaggs School of Pharmacy and Pharmaceutical Sciences, University of California, San Diego, La Jolla, CA 92093, USA

[2]Collaborative Mass Spectrometry Innovation Center, University of California, San Diego, La Jolla, CA 92093, USA

[3]Scripps Institution of Oceanography, University of California, San Diego, La Jolla, CA 92093, USA

[4]Institute of Inorganic and Analytical Chemistry, University of Münster, Münster, D-48149, Germany

[5]Institute of Molecular Physiology, Microbiology and Wine Research, Johannes Gutenberg University Mainz, Hanns-Dieter-Hüsch-Weg 17, Mainz D-55128, Germany

[6]Institute of Biotechnology and Drug Research (IBWF gGmbH), Johannes Gutenberg University Mainz, Hanns-Dieter-Hüsch-Weg 17, Mainz D-55128, Germany

[7]Division of Host-Microbe Systems & Therapeutics, Department of Pediatrics, University of California San Diego, La Jolla, CA 92093, USA

[8]Chiba University-University of California San Diego Center for Mucosal Immunology, Allergy, and Vaccines (CU-UCSD cMAV), La Jolla, CA 92093, United States of America

[9]Center for Microbiome Innovation, University of California, San Diego, La Jolla, CA 92093, USA

[10]Division of Biological Sciences, University of California, San Diego, La Jolla, CA 92093, USA

[11]Present affiliation: Sapient Bioanalytics, La Jolla, CA, 92093, USA

[12]Present affiliation: CMFI Cluster of Excellence, Interfaculty Institute of Microbiology and Medicine, University of Tübingen, Tübingen, 72076, Germany

[#]Correspondence to pdorrestein@health.ucsd.edu.

[*]These authors contributed equally

Author contributions: ATA, DP, RS, and PCD developed the concept. DP, JMG, IB, LA, ET, HZ, SPN, CCS, KPM, RJD, and MR cultured organisms and prepared samples. ATA, DP, and JMG ran mass spectrometry experiments. RS wrote code and provided feedback. ATA, DP analysed the data. ET, RJD, LIA, MR and PCD provided supervision and materials. ATA, DP, and PCD wrote the manuscript. All authors edited and approved the manuscript.

Competing Interests statement: PCD is a scientific advisor to Sirenas, Galileo and Cybele and co-founder and scientific advisor to Ometa and Enveda with approval by the University of California San Diego. MR is also on the scientific advisory board of Sirenas.

Author Manuscript Author Manuscript Author Manuscript Author Manuscript

Abstract

Although metals are essential for the molecular machineries of life, systematic methods for discovering metal-small molecule complexes from biological samples are limited. Here we describe a two-step native electrospray ionization-mass spectrometry method, in which post-column pH adjustment and metal-infusion are combined with ion identity molecular networking, a rule-based data analysis workflow. This method enabled the identification of metal-binding compounds in complex samples based on defined mass (*m/z*) offsets of ion species with the same chromatographic profiles. As this native electrospray metabolomics approach is suited for any liquid chromatography-mass spectrometry system to explore the binding of *any* metal, this method has the potential to become an essential strategy for elucidating metal-binding molecules in biology.

Graphical abstract

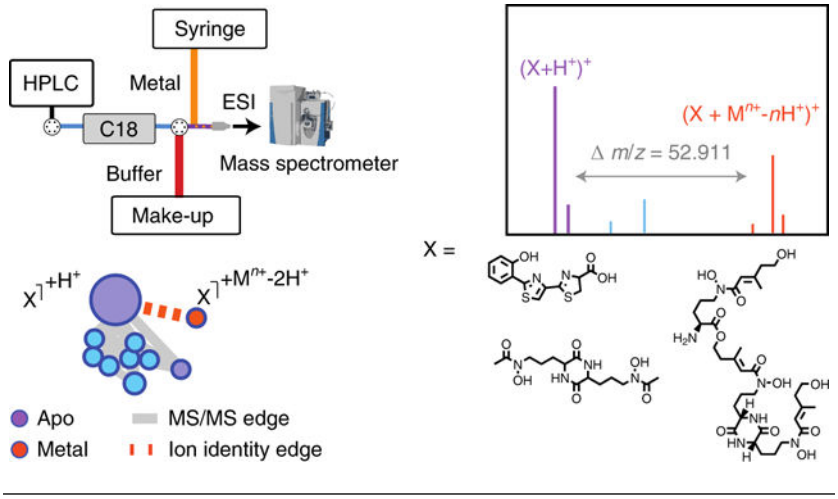

Introduction

Life, as we know it, cannot exist without metals. Metals are essential cofactors in critical biochemical reactions such as DNA replication and repair (iron and manganese), respiration (iron and copper), photosynthesis (iron and manganese), and biosynthesis of countless primary and secondary metabolites (e.g., iron, zinc, vanadium, molybdenum, magnesium, and calcium). One common strategy for metal acquisition in microorganisms is through the production and secretion of small molecule ionophores that bind metals and form noncovalent complexes. These complexes bind to specific ionophore receptors for their uptake and release of metal into the cytoplasm. Siderophores are high-affinity chelators of ferric iron (Fe^{3+}). They include ferrioxamines (i.e., desferrioxamines B and E)[1–4], catecholates (i.e., enterobactin)[1–3], and carboxylates (i.e., rhizoferrin and aerobactin)[1–4], while chalkophores such as methanobactins and SF2768 (a diisonitrile natural product) play the analogous role in binding cuprous copper (Cu^{+})[5,6]. Recently, several zincophores have also been recently elucidated[7–10]. In addition to small molecule ionophores that play a role in microbial metal transport and homeostasis, metals can also serve as cofactors essential for the function of other small molecules and proteins. Small molecule examples include

Author Manuscript Author Manuscript Author Manuscript Author Manuscript

iron in heme, magnesium in chlorophyll, calcium and magnesium in metal-dependent antibiotics[11,12], and cobalt in the vitamin cobalamin (vitamin B12); protein examples range from DNA replication and repair enzymes to oxygen transport proteins and electron transfer enzymes.

Although metal-binding small molecules have various biological functions and many potential biomedical applications, it is currently challenging to find metal-binding compounds present in complex mixtures such as microbial culture extracts[13], dissolved organic matter in seawater[14], or fecal extracts[15]. Additionally, it is challenging to assess metal-binding preferences directly in these mixtures. Predictions of small molecule structures using genome mining strategies have improved tremendously in recent years[16,17]; however, predicting the selectivity and affinity of metal coordination sites is still not possible, and it is even difficult to predict whether a small molecule contains a metal-binding site[18,19]. This is because small molecule metal-binding sites are diverse and not conserved; as such, metalbinding must be experimentally established, often relying on methods such as inductively coupled plasma-mass spectrometry (ICP-MS)[20], atomic absorption spectroscopy (AAS)[21], x-ray fluorescence spectroscopy (XRF)[22], UV-visible (UV-vis) absorption spectroscopy, and nuclear magnetic resonance (NMR) spectroscopy, which are typically low-throughput, performing best on pure compounds. With each of these methods, it is difficult to understand which molecules form metal complexes within a biological matrix that contains a pool of candidate metal ions, especially when the identities of metal-binding species are not known ahead of time.

Mass spectrometry strategies, such as the use of characteristic metal isotope fingerprints, have been used to discover siderophores from complex samples. This initially facilitated the study of siderophores in seawater[23–28] and was subsequently assisted by mass defect/Kendrick analysis[29], analysis of hyperfine splitting isotope patterns[30], and the development of software packages such as ChelomEx to enable siderophore screening strategies[31–33]. Multimodal approaches have been employed combining matrix-assisted laser desorption/ionization-Fourier transform ion cyclotron resonance mass spectrometry imaging (MALDI-FT-ICR MSI)[27] with LC-ESI-MS/LC-ICP-MS[19,34] based methods. While these methods have been instrumental in the discovery of several siderophores, we hypothesized that many metal-binding compounds (and specifically those binding metals other than iron) remain undiscovered. Our hypothesis is based on a repository scale analysis of the presence of apo (unbound) versus holo (bound) ionophores in public datasets hosted in the Global Natural Products Social (GNPS) Molecular Networking platform (SI Table 1a). To discover new small molecule-metal complexes, we envisioned developing a modular and straightforward non-targeted LC-tandem mass spectrometry (LC-MS/MS) based strategy that is broadly applicable to *any* metal and makes use of a native mass spectrometry approach, which has gained momentum in the field of structural biology and intact protein analysis[35,36]. In combination with a novel computational tool - Ion Identity Molecular Networking (IIMN) that connects related compounds by correlation analysis, user-defined mass differences, and MS/MS similarity[37], this workflow enables screening for metal-binding compounds in complex biological samples. We call the experimental workflow *native electrospray metabolomics*. When combined with IIMN, this strategy facilitates finding metal-binding compounds that may be biologically relevant. A key feature that differentiates native

Author Manuscript Author Manuscript Author Manuscript Author Manuscript

metabolomics from other LC-based methods is the ability to control pH without altering chromatography. SI Table 1b highlights the critical differences between current MS-based siderophore screening strategies and the native metabolomics approach; the novelty of the native metabolomics approach lies in its broad applicability to find biologically relevant metalcomplexes associated with *any* metal (e.g., Fe, Cu, Zn, Na, and Ca) in a wide range of pH conditions and sample complexities.

Native Metabolomics Concept.

Extraction, sample preparation, and chromatography conditions typically employed for non-targeted reversed-phase LC-MS/MS-based analysis of small molecules involve low pH, high percentages of organic solvent, and low metal concentrations, which disfavour metal complexation[38,39,89]. For example, extraction of marine dissolved organic matter for non-targeted MS/MS analysis, when not explicitly designed for isolation of metal-bound organics, typically employs low pH to protonate carboxylic acids and increase SPE extraction efficiency[14]. Based on this, we hypothesized that many metal-binding compounds detected by reversed-phase (RP)-LC-MS/MS are predominantly observed in their protonated (apo) form rather than in a metal-bound form. Investigating experimental non-targeted MS/MS datasets in a repository-scale analysis of MS/MS spectra of proton- and metal-bound siderophores in the GNPS web platform[40,41] and MetaboLights repository[42] with the Mass Spectrometry Search Tool (MASST)[43] provides evidence for this assumption (SI Table 1a). When querying a list of known siderophores (SI Table 1a) against the GNPS-MassIVE and MetaboLights repository, 73% of files contained the proton-bound form exclusively, with only 27% of files containing the metal-bound form. Notably, even when the metal-bound species is observed, it can be challenging to match it to the corresponding proton-bound species, because proton- and metal-bound species typically elute at different retention times[44–46] and exhibit significantly different MS/MS fragmentation behavior[37]. Therefore, searching for a given (metal-specific) mass (*m/z*) offset to connect proton- with metal-bound species can be non-trivial with current tools.

Given these inherent limitations of contemporary RP-LC-MS/MS methods, we hypothesized that adjusting pH to physiological values - an approach often applied in intact protein mass spectrometry that has been termed native spray[28–30] – would help to detect compounds with metal binding affinities in metabolomics experiments. Native electrospray metabolomics facilitates the ability to control pH without altering chromatography, which is not possible with other LC-based methods that aim to identify metal-binding molecules. Preliminary direct injection experiments at acidic, neutral, and basic pH showed higher ratios of metal-adduct to proton-adduct at higher pH values, which is consistent with literature[38,39,89,90,95]. Thus, we developed a two-step native electrospray ionization (ESI) LC-MS/MS workflow with online post-column pH adjustment is coupled to metal infusion to directly detect candidate small molecules that bind metals. While ion-addition has been utilized for various MS applications[47–50], the use of post-LC metal-addition for finding biologically relevant metal-binding molecules and integration of this into a widely used web-based analysis ecosystem is unique.

Author Manuscript Author Manuscript Author Manuscript Author Manuscript

Our first-generation workflow utilizes a double-barrel syringe pump for infusion of ammonium hydroxide solution and subsequent injection of one or multiple metal salt(s) (SI Figure 1a). As metal-binding kinetics are fast (on the order of milliseconds[51–54]), we hypothesized that our set-up would allow for sufficient time to establish metal-ligand complexes after chromatography, pH adjustment, and metal infusion, as it takes c.a. 0.6 seconds to reach the entrance of the electrospray inlet after the post-column metal addition. The second-generation of our workflow makes use of a secondary high-performance liquid chromatography (HPLC) pump that provides an ammonium acetate buffered make-up flow and the syringe pump delivers metal solution (Figure 1a, SI Figure 1b). This workflow offers the advantage of a more consistent (and higher percentage aqueous) solvent composition across the entire LC gradient. Based on this, the second-generation workflow was used to assess the effect of pH adjustment on metal-binding. Mixtures of metal salts - $FeCl_3$, $Cu(OAc)_2 \cdot (H_2O)$, $Mn(OAc)_2 \cdot 4(H_2O)$, $Zn(OAc)_2 \cdot 2(H_2O)$, $Co(OAc)_2 \cdot 4(H_2O)$, and $NiCl_2$ - were infused at two concentrations and at three pH values, namely pH 2, 5, and 9. The ratio of the integrated peak area of Fe-adducts, for example, to the integrated peak area of Hadducts increased at higher pH values (SI Figure 2). Based on this observation, we chose to carry out subsequent studies at pH values greater than 5, and we aimed to operate at the relevant pH value for the biological systems under investigation. While the post-LC pH was verified, ESI-induced changes in pH can occur in the ESI source[91,92,95].

Using both first and second-generation set-ups, proton- and metal-bound complexes are observed at the same retention time with the same peak shape; however, one of the critical challenges in developing this method was how to identify metal-binding complexes within large datasets and/or complex mixtures that typically contain thousands of features. The rule-based informatic workflow IIMN was used to overcome this limitation (Figure 1b) by applying MS data processing in MZmine[41,42] linked to GNPS[43,44]. Using ion identity networking (IIN) in MZmine 2, LC-MS features, defined here as chromatographic peaks with a specific *m/z*, are grouped based on their retention time and chromatographic feature shape correlation and identified as specific ion types of the same analyte molecule akin to the way it is accomplished by CAMERA[55] or RAMClust[56]. In this process, all metal-binding small molecules can be identified by linking the metal-bound ions to other adducts and in-source fragments of the apo structures. The connected ion features are then further linked within the molecular network created based on MS/MS similarity. The use of molecular networking based on MS/MS similarity facilitates dereplication of potential metal-binding compounds, i.e., a known siderophore that shares an MS/MS similarity edge with an unknown metal-binding node can be used to dereplicate the unknown metal-binding derivative[57]. Given this, we expect molecular networking will enable dereplication of many metal-binding molecules, as microbial gene clusters can make a series of small molecules in addition to their characterized small molecules product due to multiple substrate pools and promiscuity of the biosynthesis[58]. As such, IIMN is performed by (1) feature finding in MZmine 2[41,42], (2) grouping of co-occurring features using Pearson correlation of their corresponding intensity profiles, (3) filtering results based on user-defined ion rules and *m/z* error tolerances, and (4) connection of similar MS/MS spectra in GNPS through the cosine similarity metric. This enables the visualization of apo versus metal-bound compounds, even

Author Manuscript Author Manuscript Author Manuscript Author Manuscript

when the corresponding ion adducts have different gas-phase fragmentation behaviour in collision induced dissociation (SI Figure 3).

After performing feature finding that considers grouping based on feature shapes correlation in MZmine 2[41,42], all grouped features are searched in pairs against a user-defined ion identity library specified by lists of adducts, in-source fragments, and multimers. This approach tests all possible combinations of ion identities that point to the same neutral mass of an ionophore (M). All metal adducts and ion species combinations are searched, which can be crucial if no protonated feature is observed. Consequently, as proton- and metal-bound species have the same retention time (RT) and feature shape in this workflow, IIN enables discovering novel metal-binding molecules by any combination of singly or multiply charged ion species and therefore lifts any restrictions to the most common ion types. This computational workflow facilitates the search for any characteristic *m/z* delta, defined by the user, to enable finding molecules that form complexes with iron (3+ ion, *m/z* delta=52.9115), in addition to other metals such as zinc (2+ ion, 62.9208), copper (2+ ion, 61.9212), cobalt (2+ ion, 57.9248), sodium (1+, 22.9892), potassium (1+, 38.9632), calcium (2+, 39.9615), aluminium (3+, 24.9653), etc. Although alkali metals and alkaline earth metals (such as Na^+, K^+, and Ca^{2+}) are generally considered nuisances in mass spectrometry, these adduction events may also have biological relevance[59–61] and can serve as a starting point for hypothesis generation.

Results and Discussion

Metal-binding specificity.

To evaluate our native metabolomics workflow, we prepared standard mixtures of commercially available, well-characterized[94] siderophores, namely yersiniabactin (**1**), vibriobactin (**2**), enterobactin (**3**), ferrichrome (**7**), and rhodotorulic acid (**6**). The standards were separated by HPLC then subjected to post-LC pH adjustment and excess (millimolar) infusion of iron chloride ($FeCl_3$) via the first-generation set-up. We observed the Fe^{3+}-adduct of each siderophore only after iron-infusion (Figure 2a). For initial screening, iron concentrations between 3–5 mM were infused, corresponding to final concentrations of 30–50 μM (SI Table 2) at the electrospray source, a c.a. 10-fold molar excess over siderophore concentration at the electrospray source (SI Table 2). To systematically assess whether iron-binding under these conditions is dependent on concentration and to evaluate the native electrospray metabolomics method under sub-stoichiometric (and physiological) concentrations, iron was titrated into a mixture of standards containing compounds (**3**), (**7**), (**6**), in addition to desferrioxamines E (DFE) and B (DFB). This resulted in a dose-dependent response in the ratio of integrated peak areas of Fe-adduct to H-adduct (SI Figure 4). Sub-stoichiometric iron concentrations at the ESI source (SI Table 2, based on the 51x dilution) resulted in an increase in the ratio of integrated peak areas of Fe-adducts to H-adducts (over background) from which we infer relative binding affinity. This increase is compound-dependent and likely also dependent on solvent composition, particularly the proportion of organic solvent (SI Figure 4). For this reason, we developed the second-generation set-up with an additional make-up flow pump that reduces the variation in solvent composition across the gradient and lowers the organic solvent concentration by ~50%. At

Author Manuscript Author Manuscript Author Manuscript Author Manuscript

lower metal concentrations, regular cleaning of the source and spray shield (in addition to other mass spectrometer parts) becomes increasingly important as metal salts are infused. Failure to clean the instrument can result in background signals in control (non-infusion) samples, especially when compounds bind with high affinities.

While we observed that metal-binding response is concentration-dependent, we did not observe a strong correlation between relative binding affinity and solution-phase literature K_d values[66]. We speculate this may be due to potential differences in ionization efficiencies for proton- versus metal-bound ionophores, compound-dependent reduction processes that can occur during electrospray ionization, or differences in ionization efficiencies between compounds[93]. Similar caveats have also been widely described in the context of native protein analysis by mass spectrometry[35]. Initial proof-of-concept experiments focused on siderophores (versus ionophores for non-iron metals) due to the prevalence of commercially available, well-characterized[94] iron-binding standards. To assess whether observed iron-binding was specific for known siderophores or whether non-specific adducts form after iron-infusion, we added the siderophore ferrichrome to a matrix of competing molecules without described iron-binding properties, and we found iron-adduction to be specific. This mixture was analysed using the first-generation native electrospray metabolomics workflow in the absence and presence of excess (millimolar) iron. In this experiment, ferrichrome is the only compound connected with an IIMN-edge corresponding to iron-binding and no other molecules were observed to bind iron (Figure 2b).

To compare the effectiveness of native electrospray as an approach to identify small molecule-metal interactions, we compared native electrospray metabolomics to other LCMS-based siderophore screening strategies[31–33] (SI Table 1b). While these strategies can reproducibly identify iron-binding of strong siderophores, they are less suited to detect the metal adduct of compounds with low metal affinities, missed metal adducts in complex mixtures, and overlooked adducts of non-iron metals (SI Figure 5), as highlighted in the following sections of the text.

Metal-binding selectivity.

In addition to testing specificity, i.e., the ability of native metabolomics to detect only true metal-binding molecules - we next tested whether native metabolomics could be used to understand the selectivity of metal-binding. We assessed this by infusing a mixture of metals at physiological levels (μM), including iron, copper, cobalt, nickel, zinc, and manganese salts, and found that metal selectivity differed among the tested standards tested (SI Figure 2). For example, only in the case of yersiniabactin did copper-binding strongly compete with iron-binding[67]. For metal selectivity, relative binding affinities were consistent with literature that suggests yersiniabactin can bind copper more strongly than iron under certain conditions[67]. Both ferrioxamines showed a higher preference for iron than other infused metal salts; interestingly, the native metabolomics method can differentiate binding preferences of two very similar compounds, namely desferrioxamines E and B. The fact that desferrioxamine B exhibits copper-binding while desferrioxamine E does not is also consistent with literature reports[68].

Author Manuscript Author Manuscript Author Manuscript Author Manuscript

Observing Siderophores in Culture Extracts.

To further assess selectivity within biological samples, we applied this workflow on culture extracts from *Glutamicibacter arilaitensis* JB182[69]. This microbe was previously isolated from cheese and grown here in liquid cheese media. Cheese is an iron-depleted environment, as it contains lactoferrin, an iron-binding protein that sequesters free iron[70]. Siderophore production was predicted based on genomic data mining using antiSMASH 4.0[71], which identified biosynthetic gene clusters of ferrioxamine B and fuscachelin with 50% and 44% similarity, respectively. Using the native metabolomics workflow developed here, both apo-desferrioxamine E (DFE) and the Fe^{3+}– bound ferrioxamine E were observed from culture extracts and were connected by an iron-bindin IIMN edge; DFE was annotated by a spectral match from molecular networking in GNPS[43,44]. DFE was the only iron-binding connection observed using IIMN (Figure 3a), which illustrates the specificity of iron-binding during the post-LC infusion; none of the other molecules detected in this complex biological sample were iron-bound (Figure 3b–e).

Based on the promiscuous nature of metal-binding by yersiniabactin in both metal-selectivity experiments (Metal-binding selectivity) and in the literature[67,72], we were interested in further investigating metal-binding properties of this compound directly in culture extracts of *Escherichia coli* strain Nissle 1917 (*E. coli* Nissle, serotype O6:K5:H1) grown in M9 glucose minimal medium (SI Figure 5). Using the native metabolomics strategy, we ran supernatant extracts with post-LC pH adjustment to ~7 (based on *E. coli* cytosol pH[73,74]) in the absence and presence of (excess) iron-infusion and could identify a series of iron-binding molecules using IIMN (Figure 4a and SI Figure 6). From those compounds we could annotate yersiniabactin, aerobactin, and HPTzTn-COOH[75,89,90], a truncated derivative of yersiniabactin, and each corresponding iron-complex (Figure 4b–d). IIMN reveals several additional yersiniabactin (Figure 4b and c) and aerobactin (Figure 4d) derivatives that also bind iron, suggesting at least fifteen additional siderophores are present in this culture extract. SIRIUS 4.0[76] was used to predict molecular formulas of these compounds with manual inspection of retention times and MS/MS were manually inspected to exclude in source fragments and propose putative structures (SI Figure 7). This example illustrates the power of IIMN in the dereplication of siderophore derivatives that also bind iron as the molecules that co-network are structurally related to the siderophores produced by this organism. This indicates an essential aspect of molecular networking – its ability to identify structural similarity, where modifications are often associated with biosynthesis or metabolism[58]. An extension by C_2H_2, for example, cannot be an MS artifact, while an oxidation could be if the retention times are identical –IIMN would uncover this. Based on this, the predicted molecular formulas are tabulated in Table 1a (with retention times and possible in-source fragments tabulated in SI Table 3a).

In addition to investigating iron-binding at physiological pH ~7, we also sought to identify zinc-binding molecules in these culture extracts, as zinc-acquisition mechanisms of *E. coli* Nissle have not been fully elucidated. Evaluating zinc-binding molecules using native metabolomics yielded the novel finding that yersiniabactin along with a number of its derivatives, including HPTzTn-COOH, also bind zinc. Based on this result, we discovered that yersiniabactin facilitates *E. coli* Nissle's ability to flourish in an inflamed gut by

Author Manuscript Author Manuscript Author Manuscript Author Manuscript

evading zinc sequestration by the antimicrobial protein calprotectin[88]. To confirm the zinc-binding observed by native electrospray metabolomics, we monitored zinc-addition into pure yersiniabactin[88] and into HPTzTn-COOH (SI Figure 8) by 1D ^{1}H NMR. Changes in chemical shifts and peak broadening arise from zinc coordination, which changes the electronic environment of these protons; therefore, ^{1}H NMR studies serve as orthogonal confirmation of zinc-binding.

Given that these culture extracts contain compounds that bind various metals, these samples were valuable for investigating metal-competition at physiologically relevant metal concentrations (μM). The pH and ionic strength of the *E. coli* cytosol have been well characterized, with the intracellular pH ~7.5[73,74]. Labile Fe^{2+} and Mn^{2+} concentrations have been estimated to be 10 μM[77,78], while labile Cu^{+} and Zn^{2+} have been estimated to be 10^{-15} μM[61] and 10^{-9} μM[61], respectively. While alkali and alkaline earth metals (including Na^{+}, Ca^{+}, and K^{+}) are present in mM amounts, mM concentrations result in significant ion suppression during mass spectrometry, so only transition metals were infused at the levels listed above.

We found that metal adducts were still observed when physiologically relevant levels were infused. However, the increase in feature intensity of metal adduct-features is significantly less than the observed increase with excess iron infusion (SI Figure 9a–b). Interestingly, yersiniabactin exhibits both iron and copper-binding, even when only trace levels of copper are infused (SI Figure 9b–d). Additionally, we observe that metal reduction can occur during ESI[79] (Gianelli et al. 2001), as we detected small amounts of $[M+Fe^{2+}]^{2+}$ and $[M+Fe^{2+}-H^{+}]^{+}$ adducts in addition to the expected $[M+Fe^{3+}- 2H^{+}]^{+}$ adducts (SI Figure 10).

After illustrating the ability of native metabolomics to elucidate metal-binding molecules present in *E. coli* Nissle extracts specifically, we next tested this method on increasingly complex samples. We applied our method to fungal extracts from the wine fungus *Eutypa lata*. The *Eutypa lata* genome[80] is approximately ten times the size of the *E. coli* Nissle genome[81]. Moreover, the published *Eutypa lata* strain UCREL1 contains a predicted domain structure that matches the coprogen synthetase SSM2 from *Magnaporthe oryzae*[82,83]. Applying the post-LC pH adjustment and Fe^{3+}-infusion mass spectrometry workflow enabled the detection of apo-coprogen B and apo-hydroxydimethyl coprogen B in addition to the iron-bound forms of both siderophores. Apo and Fe^{3+}-bound forms were each connected through an Fe^{3+}-binding IIMN edge (Figure 4e). We additionally identified several structurally related derivatives in the same molecular family that bind iron (Figure 4f). As in the *E. coli* Nissle example, we used SIRIUS 4.0[76] to elucidate molecular formulas and have putatively annotated six structurally related novel siderophores, again underscoring the potential of this method for the discovery of new analogues[58,84]. These siderophores are tabulated in Table 1b (with retention times tabulated in SI Table 3b), and MS/MS spectra are annotated (SI Figure 11).

Observing Metal-Binding Molecules in Complex Environmental Samples.

Finally, we applied the native metabolomics workflow to environmental samples to test whether this workflow could identify metal-binding compounds in ultracomplex samples. We analysed solid-phase extracted surface ocean samples collected in the California Current

Author Manuscript Author Manuscript Author Manuscript Author Manuscript

Ecosystem during a phytoplankton bloom in June 2017 with our native metabolomics approach. Dissolved organic matter (DOM) from surface seawater is among the most complex samples analysed by UHPLC-MS/MS in our labs (more complex than fecal and on par with crude oil samples). Metals were infused post-column after pH adjustment to ~8 (average pH of the ocean water in California Current Ecosystem[85]). The native metabolomics method identifies domoic acid (DA) as a copper-binding molecule, which is consistent with the literature[86,87]. Furthermore, we confirmed the identity of DA as Metabolomics Standards Initiative level 1 annotation[96] with an authentic standard. Interestingly, IIMN indicated that DA binds Cu^{2+} as a dimer (Figure 5), perhaps coordinating copper in a similar binding configuration to ethylenediaminetetraacetic acid (EDTA)[91], which also contains four carboxylic acids and two amino groups that form a hexadentate complex. This example illustrates how native metabolomics can be applied to environmental samples, identifying metal-binding compounds in ultra-complex matrices.

Conclusion

The native metabolomics workflow described here can identify known and novel ionophores from complex samples, such as culture extracts and DOM. Currently, the screening for metal-binding compounds is difficult to perform on complex mixtures, as the majority of techniques used to assess metal-binding (including NMR, UV-vis, EPR) are usually performed on purified compounds. ICP-MS, ICP-OES and AAS can be used to assess bulk metal content of complex samples. However, they cannot provide molecular detail about which compounds present in a complex sample actually bind metals. Split-flow LC approaches offer innovative strategies for simultaneously analysing metal content and structures but require expensive and specialized equipment and customized set-ups[28]. Based on the minimal technical adjustments, we foresee the routine implementation of this native metal metabolomic approach into non-targeted LC-MS/MS metabolomics workflows for elucidating metal-binding small molecules in biology. Additionally, this workflow can be adapted to give detailed insights into metal-binding selectivity. Based on our results, we suspect that molecules traditionally described as iron-binding siderophores may also be responsible for binding and uptake of other metals, as we recently discovered in the case of yersiniabactin and its derivative HPTzTn-COOH; yersiniabactin has been shown to play a biological role in microbial zinc-acquisition[88]. The method outlined here is uniquely set up to identify novel metal-binding molecules in complex samples. We anticipate this will significantly improve our understanding of the role of metals across diverse fields ranging from human health to agriculture to the environment.

Online Methods

Sample Preparation.

Commercial siderophore standards were purchased from EMC Microcollections (https://www.microcollections.de/product-services/siderophores.html). Domoic acid standards were purchased from Sigma Aldrich. Standards were diluted in either water or methanol to a concentration of 1 mM and diluted further from the stock solution.

Author Manuscript Author Manuscript Author Manuscript Author Manuscript

Direct Injection MS data acquisition.

For MS analysis, 5 μL were directly infused into a Q-Exactive orbitrap mass spectrometer via flow injections through a Vanquish UHPLC system (Thermo Fisher Scientific, Bremen, Germany). A flow rate between 0.2 mL/min and 0.4 mL/min was used. MS^1 data acquisition was performed in positive mode. Electrospray ionization (ESI) parameters were set to 53 L/min sheath gas flow, 14 L/min auxiliary gas flow, 0 L/min sweep gas flow, and 400°C auxiliary gas temperature. The spray voltage was set to 3.5 kV and the inlet capillary to 320°C. 50 V S-lens level was applied. MS scan range was set to 150–1500 m/z with a resolution at m/z 200 ($R_{m/z\ 200}$) of 35,000 with one micro-scan. The maximum ion injection time was set to 100 ms with an automated gain control (AGC) target of 1.0E6.

Standard-flow LC-MS/MS data acquisition.

2–5 μL were injected into a Vanquish HPLC system coupled to a Q-Exactive orbitrap mass spectrometer (Thermo Fisher Scientific, Bremen, Germany). A C18 porous core column (Kinetex C18, 50 × 2 mm, 1.8 um particle size, 100 A pore size, Phenomenex, Torrance, USA) was used for chromatography. For gradient elution, a high-pressure binary gradient system was used. The mobile phase consisted of solvent A H_2O + 0.1 % formic acid (FA) and solvent B acetonitrile (ACN) + 0.1 % FA, unless otherwise specified. The flow rate was set to 0.5 mL/min, unless otherwise specified. One of the following two methods (*method 1* or *method 2*) was used for analysis. After injection, the samples were eluted with one of the following linear gradients: 0–0.5 min, 5% B, 0.5–5 min 5–99% B, followed by a 2 min washout phase at 99% B and a 3 min re-equilibration phase at 5% B (*method 1*) or 0–0.5 min, 5 % B, 0.5–9 min 5–100% B, followed by a 2 min washout phase at 99% B and a 3 min re-equilibration phase at 5% B (*method 2*). Data-dependent acquisition (DDA) of MS/MS spectra was performed in positive mode. ESI parameters were set to 53 L/min sheath gas flow, 14 L/min auxiliary gas flow, 0 L/min sweep gas flow, and 400°C auxiliary gas temperature, the spray voltage was set to 3.5 kV and the inlet capillary to 320°C and 50 V S-lens level was applied (*method 1*); or 60 L/min sheath gas flow, 20 L/min auxiliary gas flow, 3 L/min sweep gas flow, and 300°C auxiliary gas temperature, the spray voltage was set to 3.5 kV and the inlet capillary to 380°C and 60 V Slens level was applied (*method 2*). MS scan range was set to 150–1500 m/z with a resolution at m/z 200 ($R_{m/z\ 200}$) of 35,000 with one micro-scan. The maximum ion injection time was set to 100 ms with an automated gain control (AGC) target of 1.0E6. Up to 5 MS/MS spectra per MS1 survey scan were recorded DDA mode with $R_{m/z\ 200}$ of 17,500 with one micro-scan. The maximum ion injection time for MS/MS scans was set to 100 ms with an AGC target of 1E6 ions (*method 1*) or 5E5 ions (*method 2*). The MS/MS precursor isolation window was set to m/z 1 (*method 1*) or 2 (*method 2*). The normalized collision energy was set to a stepwise increase from 20 to 30 to 40% with z = 1 as default charge state. MS/MS scans were triggered at the apex of chromatographic peaks within 2 to 15 s from their first occurrence. Dynamic precursor exclusion was set to 5 s (*method 1*) or 30 s (*method 2*). Ions with unassigned charge states were excluded from MS/MS acquisition as well as isotope peaks.

Author Manuscript Author Manuscript Author Manuscript Author Manuscript

Micro-flow LC-MS/MS data acquisition.

For micro-flow HPLC-MS/MS analysis extracts and DOM samples were re-dissolved in methanol/water/ formic acid (80:19:1, Fisher Scientific, San Diego, USA) and 2–10 μL were injected into vanquish UHPLC system coupled to a Q-Exactive quadrupole orbitrap mass spectrometer (Thermo Fisher Scientific, Bremen, Germany) with an Agilent 1260 quaternary HPLC pump (Agilent, Santa Clara, USA) as a make-up pump. For reversed-phase chromatographic, a C18 core-shell microflow column (Kinetex C18, 150 × 1 mm, 1.8 um particle size, 100 A pore size, Phenomenex, Torrance, USA) was used. The mobile phase consisted of solvent A (H_2O + 0.1 % formic acid (FA)) and solvent B (acetonitrile (ACN) + 0.1 % FA). The flow rate was set to 100 μL/min. A linear gradient from 5–50 % B between 0–8 min and 50–99 % B between 8 and 10 min, followed by a 2 min washout phase at 99% B and a 6 min re-equilibration phase at 5 % B. Data-dependent acquisition (DDA) of MS/MS spectra was performed in positive mode. Make-up flow of ammonium acetate buffer (10 mM) was set to 100 μL/min and infused post-column through a peak T-splitter. Metal-mixture (at the concentration specified in SI Methods) was infused post-column and post-make-up through a second T-splitter at a flow rate of 5 μL/min. ESI parameters were set to 40 arbitrary units (AU) sheath gas flow, auxiliary gas flow was set to 10 AU and sweep gas flow was set to 0 AU. Auxiliary gas temperature was set to 400 °C. The spray voltage was set to 3.5 kV and the inlet capillary was heated to 320 °C. S-lens level was set to 70 V applied. MS scan range was set to 2002000 m/z with a resolution at m/z 200 ($R_{m/z\ 200}$) of 70,000 with one micro-scan. The maximum ion injection time was set to 100 ms with automatic gain control (AGC) target of 5E5. Up to two MS/MS spectra per duty cycle were acquired at $R_{m/z\ 200}$ 17,000 with one micro-scan. The maximum ion injection time for MS/MS scans was set to 100 ms with an AGC target of 5.0E5 ions and a minimum 5% AGC. The MS/MS precursor isolation window was set to m/z 1. The normalized collision energy was stepped from 20 to 30 to 40% with z = 1 as the default charge state. MS/MS scans were triggered at the apex of chromatographic peaks within 2 to 15 s from their first occurrence. Dynamic precursor exclusion was set to 5 s. Ions with unassigned charge states were excluded from MS/MS acquisition as well as isotope peaks.

Data analysis.

Feature finding and ion identity networking were performed using an in-House modified version of MZmine2.37[40–42], corr.17.7 available at https://mzmine.github.io/iin_fbmn. Feature tables, MS/MS spectra files (mgf), and ion identity networking results were exported, uploaded to MassIVE, and submitted to GNPS for feature-based molecular networking analysis. Details of the analysis are provided in the Supplementary Methods.

Data and software availability.

The data supporting the findings of this study are available within the paper and its Supplementary Information. All mass spectrometry .raw and centroided .mzXML or .mzML files are publicly available in the mass spectrometry interactive virtual environment (MassIVE) under massive.ucsd.edu with project identifier MSV000084237, MSV000085669, MSV000085206 (Standards), MSV000084289 (Cheese siderophores), MSV000082999 and MSV000084030 (Fungal siderophores),

Author Manuscript Author Manuscript Author Manuscript Author Manuscript

MSV000083387 (*E.coli* Nissle siderophores), MSV000085554 (California Current Ecosystem phytoplankton bloom samples), MSV000086744 (Chelomics vs Native Metabolomics Comparison). Ion Identity Molecular Networks (IIMN) can be accessed through gnps.ucsd.edu under direct links: https://gnps.ucsd.edu/ProteoSAFe/status.jsp?task=79d0f380b4814ff9a720836c5570036f, https://gnps.ucsd.edu/ProteoSAFe/status.jsp?task=ad4b2665dfb744d09a9d2445f1213720, https://gnps.ucsd.edu/ProteoSAFe/status.jsp?task=5459d22126e843a3a1449f8362cd267f, http://gnps.ucsd.edu/ProteoSAFe/status.jsp?task=1c3e79f0ab984386bd468e2d163281e0, https://gnps.ucsd.edu/ProteoSAFe/index.jsp?task=196a29a94c2f4c788e204b9934ea4d9b, http://gnps.ucsd.edu/ProteoSAFe/status.jsp?task=256ba734f4334c1c90f65ffbd9141d0e, https://gnps.ucsd.edu/ProteoSAFe/status.jsp?task=042939579da64e029a8b5caef8f7f2a8.

Code availability statement

The modified version of MZmine 2 (2.37, corr.17.7)[40–42] can be found here https://mzmine.github.io/iin_fbmn. GNPS[43,44] can be accessed here https://gnps.ucsd.edu/ProteoSAFe/static/gnps-splash.jsp Cytoscape[59] version 3.7.1 can be accessed here https://cytoscape.org/.

Supplementary Material

Refer to Web version on PubMed Central for supplementary material.

Acknowledgments:

Work in the PCD lab was supported by P41-GM103484, GMS10RR029121, and the Betty and Gordon Moore Foundation – these funding sources supported ATA. DP was supported through the Deutsche Forschungsgemeinschaft with grant PE 2600/1. Work in MR lab is supported by Public Health Service Grants AI126277, AI114625, AI145325, by the Chiba University-UCSD Center for Mucosal Immunology, Allergy, and Vaccines, and by the UCSD Department of Pediatrics – these sources supported HZ and SPN. MR also holds an Investigator in the Pathogenesis of Infectious Disease Award from the Burroughs Wellcome Fund. Work in the RJD lab is supported by NIH 1 DP2 AT010401-01 – these sources supported KPM and CCS. Additionally, we would like to thank Drs. Alan Jarmusch and Scott McLuckey for helpful discussions, and we would like to thank Dr. Brendan Duggan for helpful discussion and assistance with NMR experiments.

References

1. Holden VI & Bachman MA Diverging roles of bacterial siderophores during infection. Metallomics 7, 986–995 (2015). [PubMed: 25745886]
2. Sandy M. & Butler A. Microbial Iron Acquisition: Marine and Terrestrial Siderophores. Chem Rev. 109, 4580–4595 (2009). [PubMed: 19772347]
3. Raymond KN, Allred BE & Sia AK Coordination Chemistry of Microbial Iron Transport. Acc. Chem. Res. 48, 2496–2505 (2015). [PubMed: 26332443]
4. Vraspir JM & Butler A. Chemistry of Marine Ligands and Siderophores. Annu. Rev. Mar. Sci 1, 43–63 (2009).
5. Kenney GE & Rosenzweig AC Chalkophores. Annu. Rev. Biochem. 87, 645–676 (2018). [PubMed: 29668305]
6. Wang L. et al. Diisonitrile Natural Product SF2768 Functions as a Chalkophore That Mediates Copper Acquisition in Streptomyces thioluteus. ACS Chem Biol. 12, 3067–3075 (2017). [PubMed: 29131568]
7. Johnstone TC & Nolan EM Beyond Iron: Non-Classical Biological Functions of Bacterial Siderophores. Dalton Trans. 44, 6320–6339 (2015). [PubMed: 25764171]

Author Manuscript Author Manuscript Author Manuscript Author Manuscript

8. Łobodaa D. & Rowińska-Żyrek M. Zinc binding sites in Pra1, a zincophore from Candida albicans. Dalton Trans. 46, 13695–13703 (2017). [PubMed: 28725901]
9. Wilson D, Citiulo F. & Hube B. Zinc Exploitation by Pathogenic Fungi. PLOS Pathog 8, e1003034 (2012).
10. Capdevila DA, Wang J. & Giedroc DP Bacterial Strategies to Maintain Zinc Metallostasis at the Host-Pathogen Interface. J. Biol. Chem. 291, 20858–20868 (2016).
11. Hover BM et al. Culture-independent discovery of the malacidins as calciumdependent antibiotics with activity against multidrug-resistant Gram-positive pathogens. Nat. Microbiol 3, 415–422 (2018). [PubMed: 29434326]
12. Wood TM & Martin NI The calcium-dependent lipopeptide antibiotics: structure, mechanism, & medicinal chemistry. Med. Chem. Commun 10, 634–646 (2019).
13. von Eckardstein L. et al. Total Synthesis and Biological Assessment of Novel Albicidins Discovered by Mass Spectrometric Networking. Chem.: Eur. J. 23, 15316–15321 (2017). [PubMed: 28876492]
14. Petras D. et al. High-Resolution Liquid Chromatography Tandem Mass Spectrometry Enables Large Scale Molecular Characterization of Dissolved Organic Matter. Front. Mar. Sci, doi: 10.3389/fmars.2017.00405 (2017).
15. Gauglitz JM Reference data based insights expand understanding of human metabolomes. BioRxiv, doi:10.1101/2020.07.08.194159 (2020).
16. Medema MH & Fischbach MA Computational approaches to natural product discovery. Nat Chem Biol. 11, 639–648 (2015). [PubMed: 26284671]
17. Bachmann BO, Van Lanene SG & Baltz RH Microbial genome mining for accelerated natural products discovery: is a renaissance in the making? J. Ind. Microbiol. Biotechnol. 41, 175–184 (2014). [PubMed: 24342967]
18. Kasampalidis IN, Pitas I. & Lyroudia K. Conservation of metal-coordinating residues. Proteins: Struct. Funct. Bioinf 68, 123–130 (2007).
19. Cvetkovic A. et al. Microbial metalloproteomes are largely uncharacterized. Nature 466, 779–782 (2010). [PubMed: 20639861]
20. Ackerman CM, Lee S. & Chang CJ Analytical Methods for Imaging Metals in Biology: From Transition Metal Metabolism to Transition Metal Signaling. Analytical Chemistry 89, 22–41, doi:10.1021/acs.analchem.6b04631 (2017). [PubMed: 27976855]
21. Piper KG & Higgins G. Estimation of Trace Metals in Biological Material by Atomic Absorption Spectrophotometry. Proc. Ass. Clin. Biochem. 4, 190–197 (1967).
22. Aschner M. et al. Imaging metals in Caenorhabditis elegans. Metallomics 9, 357–364 (2017). [PubMed: 28054081]
23. Mawji E. et al. Production of siderophore type chelates in Atlantic Ocean waters enriched with different carbon and nitrogen sources. Mar. Chem. 124, 90–99 (2011).
24. Mawji E. et al. Hydroxamate siderophores: occurrence and importance in the Atlantic Ocean. Environ. Sci. Technol. 42, 8675–8680 (2008). [PubMed: 19192780]
25. Gledhill M. et al. Production of siderophore type chelates by mixed bacterioplankton populations in nutrient enriched seawater incubations. Mar. Chem. 88, 75–83 (2004).
26. Velasquez I. et al. Detection of hydroxamate siderophores in coastal and SubAntarctic waters off the South Eastern Coast of New Zealand. Mar. Chem. 126, 97107 (2011).
27. Boiteau RM & Repeta DJ An extended siderophore suite from Synechococcus sp. PCC 7002 revealed by LC-ICPMS-ESIMS. Metallomics 7, 877–884 (2015). [PubMed: 25786191]
28. Boiteau RM et al. Siderophore-based microbial adaptations to iron scarcity across the eastern Pacific Ocean. Proc. Nat. Acad. Sci. USA 113, 14237–14242 (2016). [PubMed: 27911777]
29. Pluháček T. et al. Characterization of microbial siderophores by mass spectrometry. Mass Spectrom. Rev. 35, 35–47 (2016). [PubMed: 25980644]
30. Walker LR et al. Unambiguous identification and discovery of bacterial siderophores by direct injection 21 Tesla Fourier transform ion cyclotron resonance mass spectrometry. Metallomics 9, 82–92 (2017). [PubMed: 27905613]

Author Manuscript Author Manuscript Author Manuscript Author Manuscript

31. Baars O, Zhang X, Morel FM & Seyedsayamdost MR The Siderophore Metabolome of Azotobacter vinelandii. Appl. Environ. Microbiol. 82, 27–39 (2015). [PubMed: 26452553]
32. Baars O, Morel FMM & Perlman DH ChelomEx: isotope-assisted discovery of metal chelates in complex media using high-resolution LC-MS. Anal Chem 86, 11298–11305 (2014). [PubMed: 25333600]
33. Baars O. et al. Crochelins: Siderophores with an Unprecedented Iron-Chelating Moiety from the Nitrogen-Fixing Bacterium Azotobacter chroococcum. Angew. Chem. Int. Ed. 130, 545–550 (2018).
34. Garcia-Sartal C. et al. Two-dimensional HPLC coupled to ICP-MS and electrospray ionisation (ESI)-MS/MS for investigating the bioavailability in vitro of arsenic species from edible seaweed. Anal and Bioanal. Chem. 402, 3359–3369 (2012). [PubMed: 22012212]
35. Leney AC & Heck AJR Native Mass Spectrometry: What is in the Name? J. Am. Soc. Mass Spectrom. 28, 5–13 (2017).
36. Heck AJR Native mass spectrometry: a bridge between interactomics and structural biology. Nat. Methods 5, 927–933 (2008). [PubMed: 18974734]
37. Schmid R. et al. Ion Identity Molecular Networking in the GNPS Environment. Nat. Comm. 12, 3832 (2021).
38. Ross ARS, Ikonomou MG & Orians KJ Electrospray ionization of alkali and alkaline earth metal species. Electrochemical oxidation and pH effects. J. Mass Spectrom. 35, 981–989 (2000). [PubMed: 10972998]
39. Lopes NP, Stark CBW, Hong H, Gates PJ & Stauntona J. A study of the effect of pH, solvent system, cone potential and the addition of crown ethers on the formation of the monensin protonated parent ion in electrospray mass spectrometry. Analyst 126, 1630–1632 (2001).
40. Wang M. Sharing and community curation of mass spectrometry data with Global Natural Products Social Molecular Networking. Nat Biotechnol. 34, 828–837 (2016). [PubMed: 27504778]
41. Aron AT Reproducible molecular networking of untargeted mass spectrometry data using GNPS. Nat. Prot. 15, 1954–1991 (2020).
42. Kale NS et al. MetaboLights: An Open-Access Database Repository for Metabolomics Data. Curr. Protocols 53, 14.13.11–14.13.18 (2016).
43. Wang M. Mass spectrometry searches using MASST. Nat. Biotechnol. 38, 23–26 (2020). [PubMed: 31894142]
44. Koh E. et al. Metal selectivity by the virulence-associated yersiniabactin metallophore system. Metallomics 7, 1011–1022 (2015). [PubMed: 25824627]
45. Bae W. & Mehra RK Metal-binding characteristics of a phytochelatin analog (GluCys)2Gly. J. Inorg. Biochem. 68, 201–210 (1997).
46. Raab A, Feldmann J. & Meharg AA The Nature of Arsenic-Phytochelatin Complexes in Holcus lanatus and Pteris cretica. Plant Physiol. 134 (2004).
47. Lee SW, Kim HS & Beauchamp JL Salt Bridge Chemistry Applied to GasPhase Peptide Sequencing: Selective Fragmentation of Sodiated Gas-Phase Peptide Ions Adjacent to Aspartic Acid Residues. J. Am. Chem. Soc. 120, 3188–3195 (1998).
48. Crizer DM, Xia Y. & McLuckey SA Metal Complexes as Reagents for Peptide Anions. J. Am. Soc. Mass Spectrom. 20, 1718–1722 (2009). [PubMed: 19535265]
49. Hu P. & Loo JA Gas-Phase Coordination Properties of Zn2+, Cu2+, Ni2+, and Co2+ with Histidine-Containing Peptides. J. Am. Chem. Soc. 117, 11314–11319 (1995).
50. Bowden JA, Albert CJ, Barnaby OS & Ford DA Analysis of cholesteryl esters and diacylglycerols using lithiated adducts and electrospray ionization-tandem mass spectrometry. Anal. Biochem. 417, 202–210 (2011). [PubMed: 21741949]
51. Billo EJ, Brito KK & Wilkins RG Kinetics of Formation and Dissociation of Metallocarboxypeptidases. Bioinorg. Chem. 8, 461–475 (1978). [PubMed: 100144]
52. Magzoub M, Padmawar P, Dix JA & Verkman AS Millisecond association kinetics of K+ with triazacryptand-based K+ indicators measured by fluorescence correlation spectroscopy. J Phys Chem B. 110, 21216–21221 (2006). [PubMed: 17048948]

Author Manuscript Author Manuscript Author Manuscript Author Manuscript

53. Chock PB Relaxation Study of Complex Formation between Monovalent Cations and Cyclic Polyethers. Proc. Nat. Acad. Sci. USA 69, 1939–1942 (1972). [PubMed: 4505671]
54. Pasternack RF, Gipp L. & Sigel H. Thermodynamics and Kinetics of Complex Formation between Cobalt(II), Nickel(II), and Copper (II) with Glycyl-L-leucine and L-Leucylglycine. J. Am. Chem. Soc. 94, 8031–8038 (1972). [PubMed: 5079962]
55. Kuhl C, Tautenhahn R, Böttcherr C, Larson TR & Neumann S. CAMERA: An integrated strategy for compound spectra extraction and annotation of LC/MS data sets. Anal. Chem. 84, 283–289 (2012). [PubMed: 22111785]
56. Broeckling CD, Afsar FA, Neumann S, Ben-Hur A. & Prenni JE RAMClust: A Novel Feature Clustering Method Enables Spectral Matching-Based Annotation for Metabolomics Data. Anal. Chem. 86, 6812–6817 (2014). [PubMed: 24927477]
57. Moree W. e. a. Interkingdom metabolic transformations captured by microbial imaging mass spectrometry. Proc. Nat. Acad. Sci. USA 109, 13811–13816 (2012). [PubMed: 22869730]
58. Fischbach MA & Clardy J. One pathway, many products. Nat. Chem. Biol. 3, 353355 (2007).
59. Tang CY & Allen HC Ionic binding of Na+ versus K+ to the carboxylic acid headgroup of palmitic acid monolayers studied by vibrational sum frequency generation spectroscopy. J. Phys. Chem. A. 113, 7383–7393 (2009). [PubMed: 19453122]
60. Aggerholm T, Nanita SC, Koch KJ & Cooks RG Clustering of nucleosides in the presence of alkali metals: Biologically relevant quartets of guanosine, deoxyguanosine and uridine observed by ESI-MS/MS. J. Mass Spec 38, 87–97 (2003).
61. Moons R. et al. Metal ions shape α-synuclein. Sci. Reports 10, 16293 (2020).
62. Leib RD, Flick TG & Williams ER Direct Quantitation of Peptide Mixtures without Standards using Clusters Formed by Electrospray Ionization Mass Spectrometry. Anal. Chem. 81, 3965–3972 (2009). [PubMed: 19354265]
63. DeMuth JC & McLuckey SA Electrospray Droplet Exposure to Organic Vapors: Metal Ion Removal from Proteins and Protein Complexes. Anal. Chem. 87, 12101218 (2015).
64. Crizer DM, Xia Y. & McLuckey SA Transition metal complex cations as reagents for gas-phase transformation of multiply deprotonated polypeptides. J. Am. Soc. Mass Spectrom 20, 1718–1722 (2011).
65. Huang T. & McLuckeistry of Multiply Charged Bioions in Analytical Mass Spectrometry. Annual Rev. Analy, S. A. Gas-Phase Chem. Chem. 3, 365–385 (2011).
66. Harris WR, Carrano CJ & Raymond KN Coordination Chemistry of Microbial Iron Transport Compounds. 16. Isolation, Characterization, and Formation Constants of Ferric Aerobactin. J. Am. Chem. Soc. 101, 2722–2728 (1979).
67. Chaturvedi KS, Hung CS, Crowley JR, Stapleton AE & Henderson JP The siderophore yersiniabactin binds copper to protect pathogens during infection. Nat. Chem. Biol. 8, 731–736 (2012). [PubMed: 22772152]
68. Sheppard LN & Kontoghiorghes GJ Competition between deferiprone, desferrioxamine and other chelators for iron and the effect of other metals. Arzneimittelforschung 43, 659–663 (1993). [PubMed: 8352819]
69. Bonham KS, Wolfe BE & Dutton RJ Extensive horizontal gene transfer in cheese-associated bacteria. eLife 6, e22144, doi:10.7554/eLife.22144 (2017).
70. Monnet C, Back A. & Irlinger F. Growth of aerobic ripening bacteria at the cheese surface is limited by the availability of iron. Appl. Environ. Microbiol. 78, 3185–3192 (2012). [PubMed: 22367081]
71. Blin K. et al. antiSMASH 4.0—improvements in chemistry prediction and gene cluster boundary identification. Nucleic Acids Res. 45, W36–W41 (2017). [PubMed: 28460038]
72. Moscatello NJ & Pfeifer BA Yersiniabactin metal binding characterization and removal of nickel from industrial wastewater. Biotech. Prog. 33, 1548–1554 (2017).
73. Wilks JC & Slonczewski JL pH of the cytoplasm and periplasm of Escherichia coli: rapid measurement by green fluorescent protein fluorimetry. J. Bacteriol. 189, 5601–5607 (2007). [PubMed: 17545292]

Author Manuscript Author Manuscript Author Manuscript Author Manuscript

74. Slonczewski JL, Rosen BP, Alger JR & Macnab RM pH homeostasis in Escherichia coli: measurement by 31P nuclear magnetic resonance of methylphosphonate and phosphate. Proc. Nat. Acad. Sci. USA 78, 6271–6275 (1981). [PubMed: 7031646]
75. Xu G, Guo H. & Lv H. Metabolomics Assay Identified a Novel Virulence-Associated Siderophore Encoded by the High-Pathogenicity Island in Uropathogenic Escherichia coli. J. Proteome Res. 18, 2331–2336 (2019). [PubMed: 30994357]
76. Dührkop K. et al. SIRIUS 4: a rapid tool for turning tandem mass spectra into metabolite structure information. Nat. Methods 16, 299–302 (2019). [PubMed: 30886413]
77. Chandrangsu P, Rensing C. & Helmann JD Metal homeostasis and resistance in bacteria. Nat. Rev. Microbiol. 15, 338–350 (2017). [PubMed: 28344348]
78. Keyer K. & Imlay JA Inactivation of dehydratase [4Fe-4S] clusters and disruption of iron homeostasis upon cell exposure to peroxynitrite. J. Biol. Chem. 272, 27652–27659 (1997). [PubMed: 9346904]
79. Gianelli L, Amendola V, Fabbrizzi L, Pallavicini P. & Mellerio GG Investigation of reduction of Cu(II) complexes in positive-ion mode electrospray mass spectrometry. Rapid Comm. in Mass Spec. 15, 2347–2353 (2001).
80. Blanco-Ulate B, Rolshausen PE & Cantu D. Draft Genome Sequence of the Grapevine Dieback Fungus Eutypa lata UCR-EL1. Genome Announcement 1, e00228–00213 (2013).
81. Reistera M. et al. Complete genome sequence of the Gram-negative probiotic Escherichia coli strain Nissle 1917. J. Biotech. 187, 106–107 (2014).
82. Hof C, Eisfeld K, Antelo L, Foster AJ & Anke H. Siderophore synthesis in Magnaporthe grisea is essential for vegetative growth, conidiation and resistance to oxidative stress. Fungal Genet. Biol. 46, 321–332 (2009). [PubMed: 19171198]
83. Antelo L. et al. Siderophores produced by Magnaporthe grisea in the presence and absence of iron. Z Naturforsch C 61, 461–464 (2006).
84. McRose DL, Seyedsayamdost MR & Morel FMM Multiple siderophores: bug or feature? J. Biol. Inorg. Chem. 23, 983–993 (2018). [PubMed: 30264174]
85. Jiang LQ, Carter BR, Feely RA, Lauvset SK & Olsen A. Surface ocean pH and buffer capacity: past, present and future. Sci. Reports 9, 18624, doi:10.1038/s41598-019-55039-4 (2019).
86. Rue E. & Bruland K. Domoic acid binds iron and copper: a possible role for the toxin produced by the marine diatom Pseudo-nitzschia. Mar. Chem. 76, 127–134 (2001).
87. Geuer JK et al. Dissolved Domoic Acid Does Not Improve Growth Rates and Iron Content in Iron-Stressed Pseudo-Nitzschia subcurvata. Front. Mar. Sci. 7, 478 (2020).
88. Zhi H. et al. Siderophore-mediated zinc acquisition enhances enterobacterial colonization of the inflamed gut. BioRxiv, doi:10.1101/2020.07.20.212498 (2020).
89. Waska H, Koschinsky A. & Dittmar T. Fe- and Cu-Complex Formation with Artificial Ligands Investigated by Ultra-High Resolution Fourier-Transform ion Cyclotron Resonance Mass Spectrometry (FT-ICR-MS): Implications for Natural Metal-Organic Complex Studies. Front. Mar. Sci. 3, 119 (2016).
90. Rellán-Álvarez R, Abadía J. & Álvarez-Fernández A. Formation of metalnicotianamine complexes as affected by pH, ligand exchange with citrate and metal exchange. A study by electrospray ionization time-of-flight mass spectrometry. Rapid Comm. in Mass Spec. 22, 1553–1562 (2008).
91. Konermann L. Addressing a Common Misconception: Ammonium Acetate as Neutral pH “Buffer” for Native Electrospray Mass Spectrometry. J. Am. Soc. Mass Spectrom. 28, 1827–1835 (2017). [PubMed: 28710594]
92. Wang H. & Agnes GR Kinetically Labile Equilibrium Shifts Induced by the Electrospray Process. Anal. Chem. 71, 4166–4172 (1999). [PubMed: 21662847]
93. Di Marco VB, & Bombi GG Electrospray mass spectrometry (ESI-MS) in the study of metal–ligand solution equilibria. Mass Spectrom. Rev. 25, 347–379 (2006). [PubMed: 16369936]
94. Gledhill M. Electrospray ionisation-mass spectrometry of hydroxamate siderophores. The Analyst 126, 1359–1362 (2001). [PubMed: 11534605]
95. Wang H, & Agnes GR Kinetically Labile Equilibrium Shifts Induced by the Electrospray Process. Anal. Chem. 71, 4166–4172 (1999). [PubMed: 21662847]

Author Manuscript Author Manuscript Author Manuscript Author Manuscript

96. Sumner LW Proposed minimum reporting standards for chemical analysis Chemical Analysis Working Group (CAWG) Metabolomics Standards Initiative (MSI). Metabolomics. 3, 211–221 (2007) [PubMed: 24039616]

Author Manuscript Author Manuscript Author Manuscript Author Manuscript

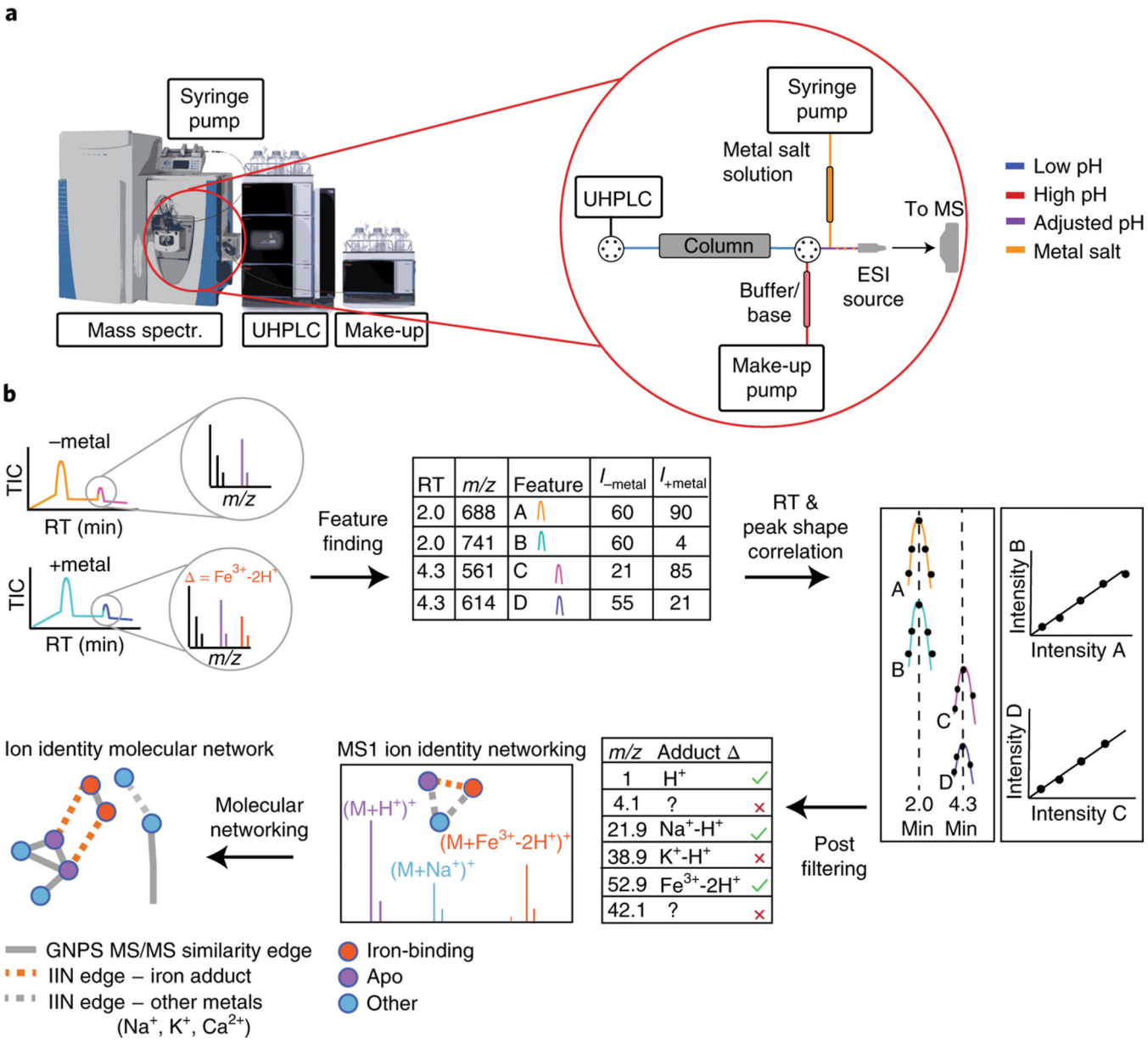

RT	*m/z*	Feature	I_{-metal}	I_{+metal}
2.0	688	A	60	90
2.0	741	B	60	4
4.3	561	C	21	85
4.3	614	D	55	21

m/z	Adduct Δ	
1	H^+	✓
4.1	?	×
21.9	Na^+-H^+	✓
38.9	K^+-H^+	×
52.9	Fe^{3+}-2H^+	✓
42.1	?	×

Figure 1. Overview of the native spray small molecule binding experiment.

(a) The two-step native ESI-MS/MS workflow utilizes a post-column infusion of ammonium hydroxide solution or ammonium acetate buffer, followed by infusion of metal salt solution (second-generation workflow shown). (b) Data can be analysed using a computational ion identity molecular networking (IIMN) workflow in MZmine and GNPS.

Author Manuscript Author Manuscript Author Manuscript Author Manuscript

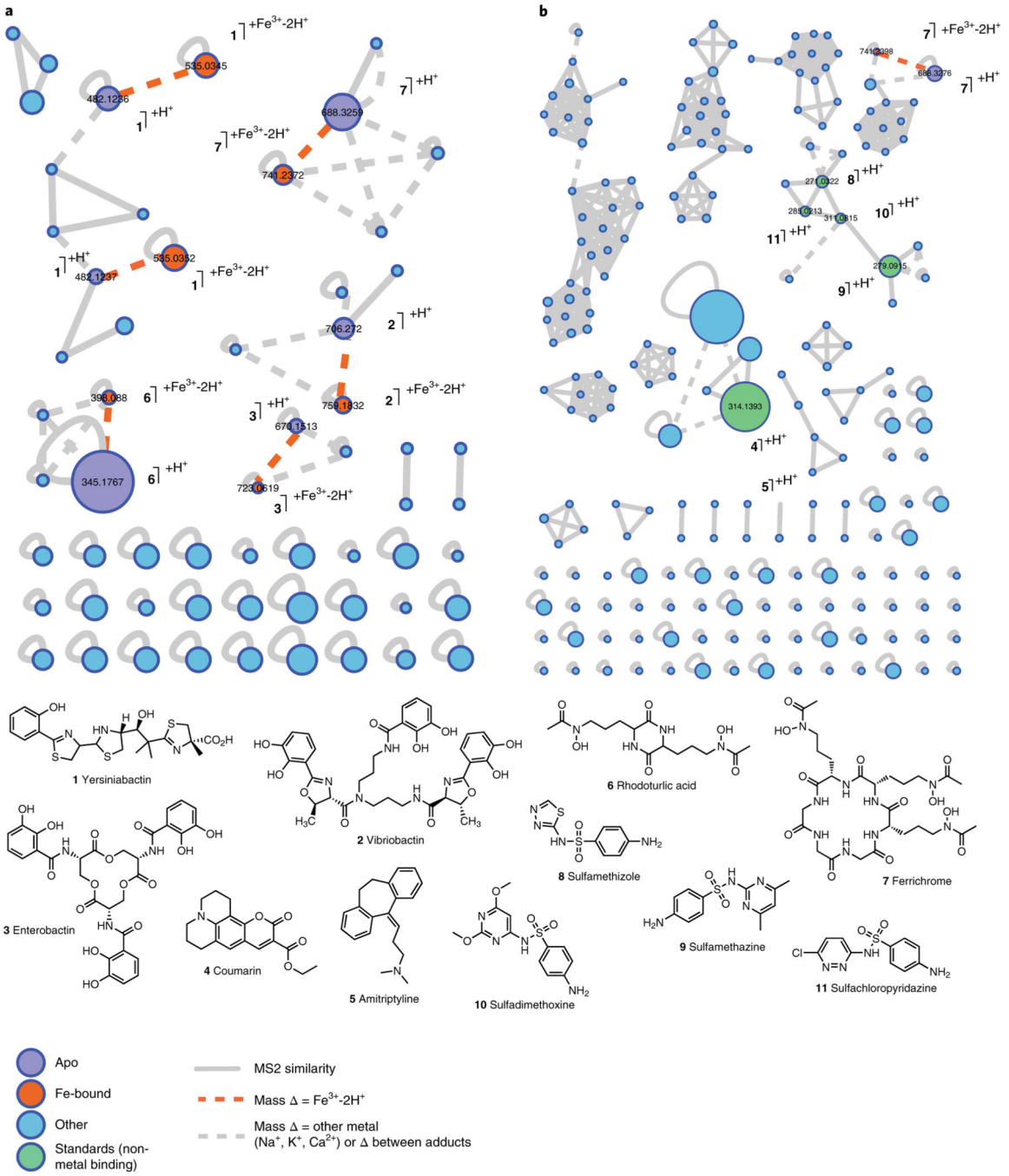

Figure 2. Post LC metal-infusion into mixtures of standards.

(a) Post-LC infusion of Fe^{3+} and post-pH adjustment of a mixture containing ionophore standards (1,2,3,6 and 7). Each of the five ionophore standards is complexed with iron (orange dashed line). (b) Post-LC infusion of Fe^{3+} and post-pH adjustment can be utilized to selectively observe the iron-bound adduct ferrichrome (7) in the presence of molecules (4,5,8,9,10, and 11), that have no reported iron-binding behaviour. Nodes corresponding to an $[M+H]^+$ ion of apo siderophores are coloured in purple and nodes corresponding to iron-bound siderophores are coloured in orange. MS/MS similarity edges are solid grey

Author Manuscript Author Manuscript Author Manuscript Author Manuscript

lines, IIN edges corresponding to an iron *m/z* delta are dashed orange lines, and IIN edges corresponding to other metals (such as Na^+, Ca^{2+}, and K^+) or *m/z* deltas between different combinations of metals are dashed grey lines. The size of the nodes corresponds to the relative area of the feature.

Author Manuscript Author Manuscript Author Manuscript Author Manuscript

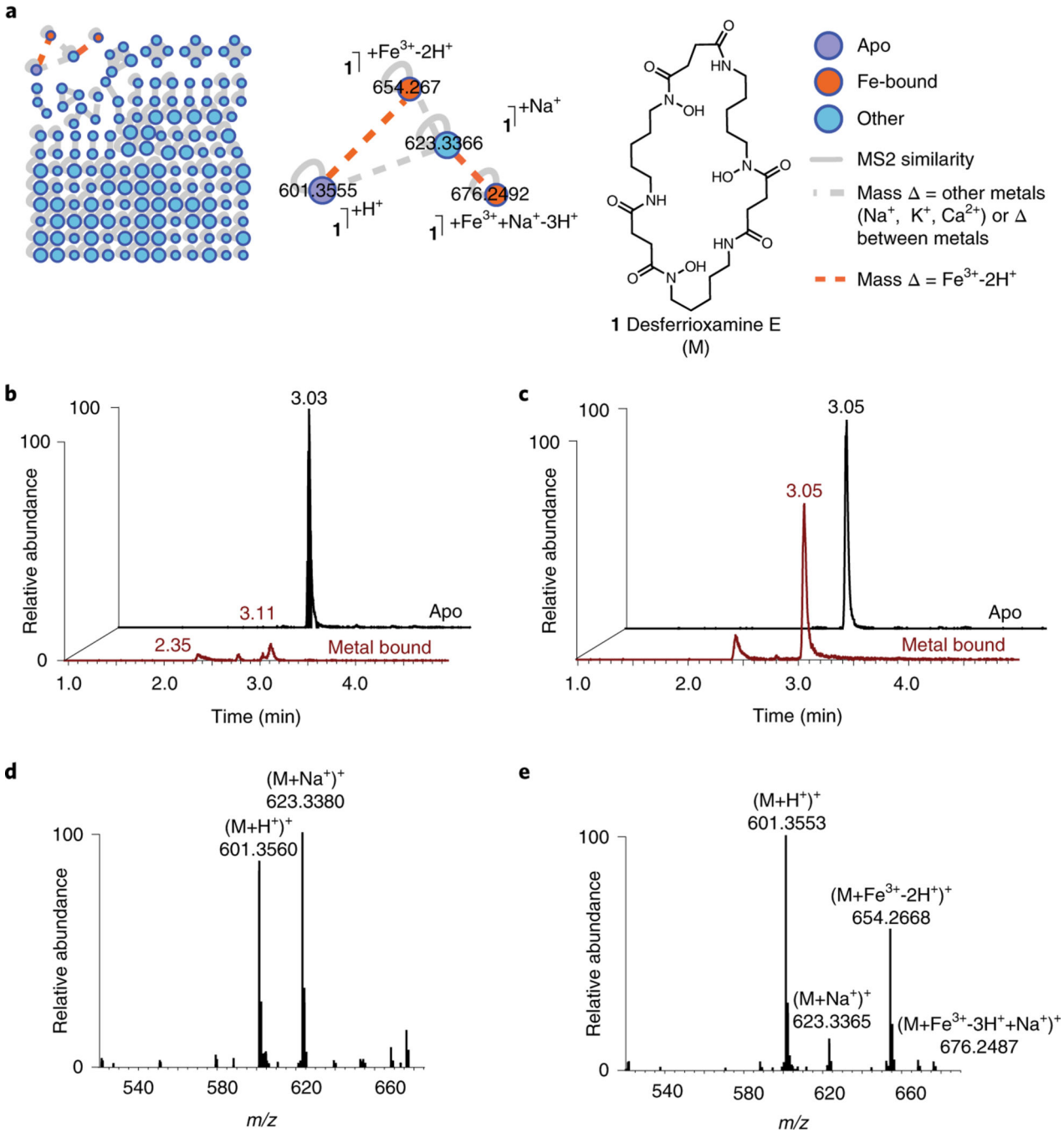

Figure 3. Native spray metal metabolomics is used to identify siderophores in bacterial culture extracts.

(a) Desferrioxamine E (DFE) is identified as the only siderophore present in *Glutamicibacter arilaitensis.* JB182 extracts. The only Fe^{3+}-binding IIN edges observed in the entire network correspond to DFE and the sodium adduct of DFE. (b) Extracted Ion Chromatogram of apo-DFE (*m/z* 601.3560, black) and Fe^{3+}-bound DFE (*m/z* 654.2668, red) when analysis is performed using standard LC-MS/MS conditions. (c) Extracted Ion Chromatogram of apo-DFE (*m/z* 601.3560, black) and Fe^{3+}-bound DFE (*m/z* 654.2668, red) when the analysis is performed using Fe^{3+}-infusion LC-MS/MS conditions. (d) MS^1 of the DFE peak (at

retention time 3.03 min) in (b). Only the apo- and Na^{+}-adduct are observed, with an *m/z* delta of 21.9819, but no Fe^{3+}-bound peak is observed. (e) MS^{1} of the DFE peak (at retention time 3.05 min) in (c). The apo- and the Fe^{3+}-bound peak are observed, with an *m/z* delta of 52.9115.

Author Manuscript Author Manuscript Author Manuscript Author Manuscript

Author Manuscript Author Manuscript Author Manuscript Author Manuscript

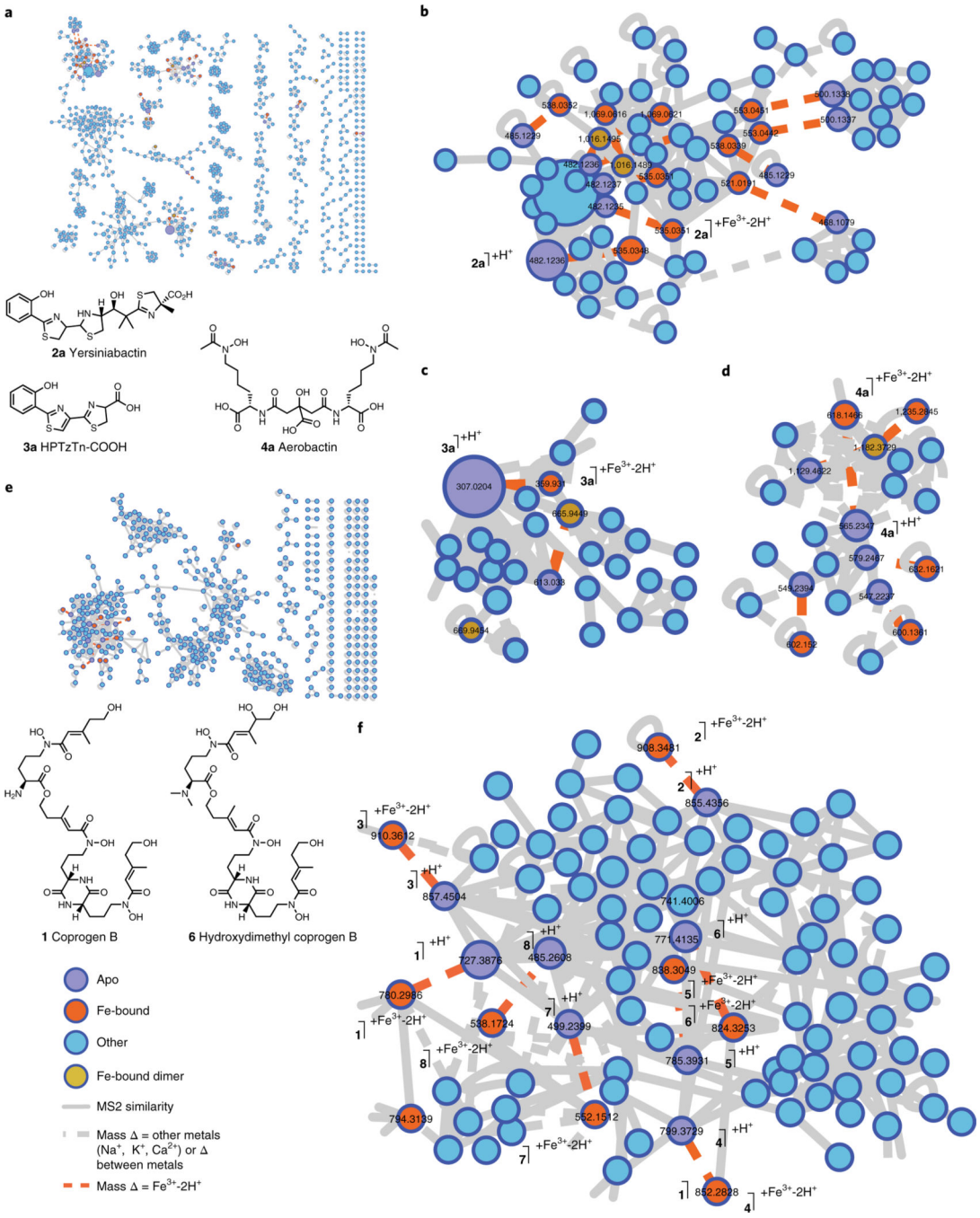

Figure 4. Native spray metal metabolomics is used to identify known and novel siderophores in bacterial and fungal culture extracts.

(a) Several siderophores are observed in *E. coli* Nissle culture extracts when a post-LC infusion of Fe^{3+} and post-pH adjustment is performed. Singleton nodes have been removed from this network. A number of (b) yersiniabactin (**2a**) derivatives, including (c) the truncated biosynthetic intermediate of yersiniabactin, HPTzTn (**3a**), in addition to (h) aerobactin (**4a**) derivatives are identified using native metal metabolomics. These derivatives are tabulated in Table 1a. (e) Several siderophores are also observed in *Eutypa lata* culture

Author Manuscript Author Manuscript Author Manuscript Author Manuscript

extracts when native metabolomics is used, (f) corresponding to coprogen B (**1**) and hydroxydimethyl coprogen B (**6**) derivatives (**2–5**, **7–8**), which are tabulated in Table 1b.

Author Manuscript Author Manuscript Author Manuscript Author Manuscript

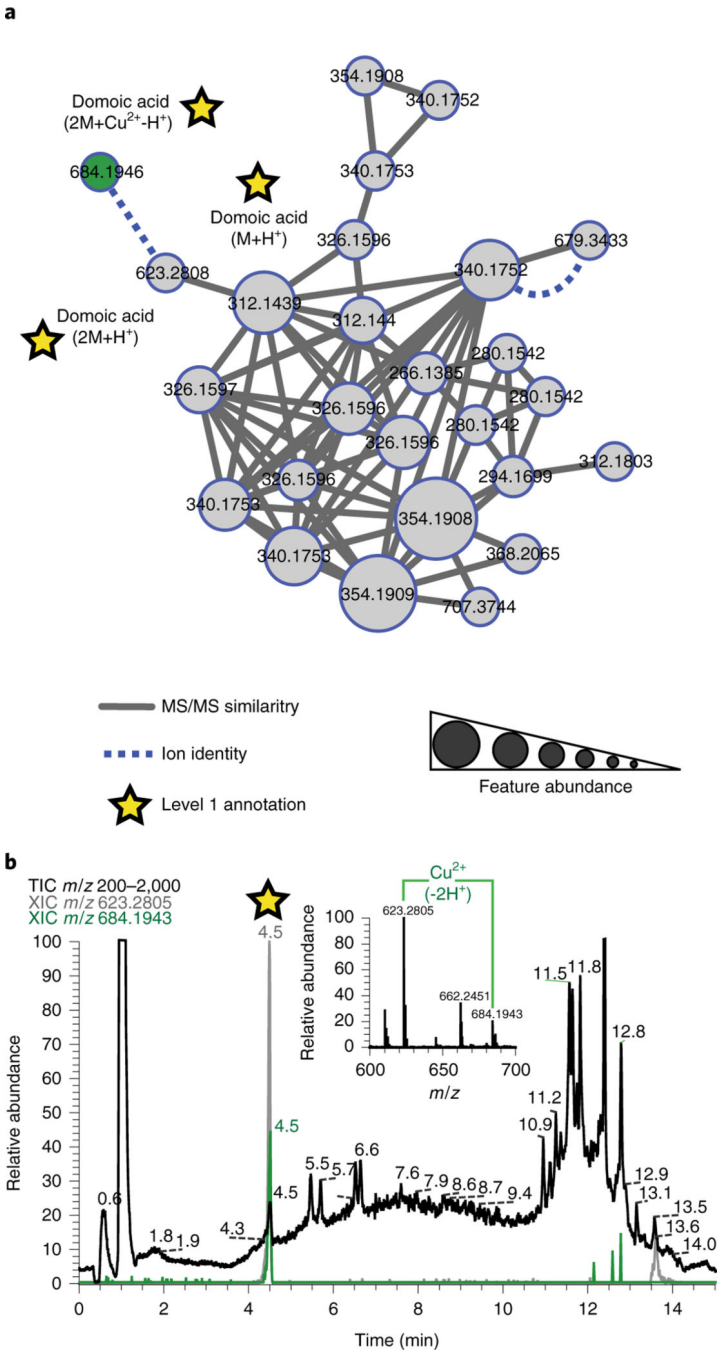

Figure 5. Native spray metal metabolomics of dissolved organic matter samples.

Surface Seawater Samples were collected in the California Current Ecosystem during a phytoplankton bloom in June 2017. (a) Ion-Identity Molecular Network of the domoic acid (DA) molecular family shows a DA dimer as well as this dimer bound to Cu^{2+}. The identity of DA was confirmed as level 1 with an authentic standard in its apo, apo-dimer and the dimerholo form. (b) Total ion chromatograms (TIC) and extracted ion chromatograms (XIC) of DA dimer and the copper-bound dimer.

Author Manuscript

Author Manuscript

Author Manuscript

Author Manuscript

Table 1.

Iron-binding derivatives identified in *E. coli* Nissle (a) and *Eutypa lata* (b) cultures have been tabulated above.

	m/z $[M+H^+]^+$	**Mol. Formula**
1a	325.0311	$C_{13}H_{12}N_2O_4S_2$
2a	482.124	C21H27N3O_4S3
3a	307.021	C13H10N2O3S2
4a	565.229	C22H36N4O13
5a	478.0921	C21H23N3O4S3
6a	468.108	C20H25N3O4S3
7a	485.116	*
8a	500.136	C21H29N3O5S3
9a	547.226	C22H34N4O12
10a	549.246	C22H36N4O12
11a	579.302	C23H38N4O13
12a	1129.462	*
13a	297.0762	C13H16N2O2S2
14a	295.0569	C13H14N2O2S2
15a	449.1187	C20H20N2O10
16a	465.1137	C20H20N2O11
17a	327.0466	C13H14N2O4S2
18a	627.167	C26H30N2O16

	m/z $[M+H^+]^+$	**Mol. Formula**
1	727.381	C33H55N6O12
2	855.437	C39H62N6O15
3	857.456	C39H64N6O15
4	799.372	C35H54N6O15
5	785.393	C35H56N6O14
6	771.41	C35H58N6O13
7	499.24	C22H34N4O9
8	485.26	C22H36N4O8

*(*)*The molecular (mol.) formula corresponds to the top-scoring formula with the top score assigned in SIRIUS 4.0[1], and those compounds with one or less matched peaks in SIRIUS 4.0 have been labelled with an asterisk.